

Mapping the field-emission tunneling barrier of organic adsorbates on tungsten

G. R. Condon^{a)} and J. A. Panitz

Department of Physics and Astronomy, University of New Mexico, Albuquerque, New Mexico 87131

(Received 1 July 1999; accepted 17 March 2000)

The field-emission tunneling barrier has been mapped for the doublet and quadruplet emission patterns associated with organic adsorbates on tungsten. The tunneling barrier was mapped by photometric probe-hole field-emission electron microscopy (PhotoFEEM). The adsorbates were deposited by evaporating a film of the molecule copper-phthalocyanine (CuPc) but it may be polymeric groups of CuPc or decomposition products. The tunneling barrier displays unexpected structures that are not seen in the corresponding field-emission images. Doublet patterns observed in the FEEM image can display singlet structures in the corresponding PhotoFEEM barrier maps. Similarly, quadruplet patterns in the FEEM image can display doublet structures in the PhotoFEEM barrier maps. This behavior is similar to supply limited tunneling previously observed in the field-emission barrier of a clean tungsten emitter. An analysis of deviations from purely linear Fowler–Nordheim behavior indicates that the observed structures arise from independent emitters that are spatially superimposed on the surface. © 2000 American Vacuum Society. [S0734-211X(00)12603-4]

I. INTRODUCTION

Imaging of organic molecules with high-resolution tunneling electron microscopies has attracted considerable interest for almost 50 years. However, the subject has also attracted an almost equal amount of controversy because of the notorious difficulties in interpreting the resulting images.^{1,2} When first studied with the field-emission electron microscope (FEEM), the imaging of molecular adsorbates was quickly abandoned because of the inability of field-emission measurements to unambiguously determine the nature of the observed patterns. Today, the imaging of individual molecules has returned to prominence with the development of the scanning tunneling microscope (STM). Although ambiguities still exist in the interpretation of molecular STM images,² significant progress has been made by modeling the surface tunneling barrier by quantum chemistry calculations. The effect of the surface tunneling barrier has often been described by an effective local work function^{3–5} although it is recognized that the observed barrier height is modified from a true work function by surface charge effects and adsorbate polarizabilities.^{3,6,7}

In this article, we present a series of experiments in which we have mapped the spatial structure of the field-emission tunneling barrier for organic adsorbates on tungsten. The adsorbates were deposited from a molecular beam of copper-phthalocyanine (CuPc) and likely consist of single CuPc molecules, multiple CuPc complexes, thermal decomposition products and contaminants. By measuring the tunneling probability independent of the supply of tunneling electrons, we can separate the contributions of the barrier and the local density of states (LDOS) to the appearance of FEEM

images.⁸ The field-emission tunneling barrier has been mapped for the characteristic doublet and quadruplet FEEM images associated with small organic adsorbates. Analogous measurements of the local tunneling probability can be made with the STM by determining the exponential variation in the tunneling current with respect to the tip-sample separation. However, attempts to extract the local barrier height (as described by the work function) from STM measurements often yield systematically low values due to tip-sample work function averaging and variations in the orientation of the local surface normal.³ The FEEM technique used in this article offers the advantage of being able to measure the tunneling barrier without the additional complications of a nearby probe electrode and has been used to measure single crystal face work functions for tungsten in good agreement with accepted values.⁸ We have observed unexpected spatial structures in the field-emission barrier that provide new information on the field-emission imaging mechanism and enable us to speculate on the origin of tunneling electrons observed in the emission patterns of molecular adsorbates.

II. EXPERIMENT

The experiments were performed with a multichannel photometric probe-hole FEEM, called the PhotoFEEM,⁸ to map the spatial structure of the field-emission tunneling barrier for CuPc adsorbed on a tungsten field emitter. By gathering a series of FEEM images as a function of voltage, we mapped the field-emission barrier across the surface by measuring the slope of the Fowler–Nordheim relation, $\ln(I/V^2)$ vs $(1/V)$ where I is the tunneling current and V is the applied voltage,^{9,10} from luminosity-voltage data for each pixel in the set of images (Fig. 1). The Fowler–Nordheim slope is used as a measure of the local tunneling probability because of its direct proportionality to the area under the tunneling barrier at the Fermi energy¹⁰ and, therefore, in the Wentzel–

^{a)}Current address: Surveillance Systems, MIT Lincoln Laboratory, 244 Wood Street, Lexington, Massachusetts 02173; electronic mail: gcondon@ll.mit.edu

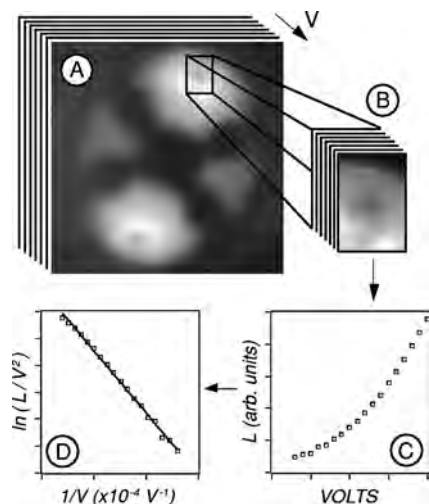


FIG. 1. Schematic illustration of the PhotoFEEM technique. (A) A series of FEEM images are taken over a range of voltages. The pixel intensities in each image are proportional to the tunneling currents at the corresponding points in the emission pattern. (B) A "virtual probe hole" of arbitrary size and shape is constructed by extracting a set of pixels from the images. (C) Luminosities, L , are obtained by integrating the pixel values over the probe hole for each voltage. (D) A Fowler-Nordheim analysis is performed on the linearized data $\ln(L/V^2)$ vs $(1/V)$.

Kramers-Brillouin (WKB) approximation, to the classical action. It is important to note that the Fowler-Nordheim slope does not measure the height of the tunneling barrier, usually described as the work function (ϕ), but is strongly dependent on it—going as $\phi^{3/2}$ for a simple Sommerfeld metal⁹ as opposed to $\phi^{1/2}$ for the tunneling barrier probed by the STM.¹¹ Since the tunneling current depends both on the local tunneling probability and on the supply of tunneling electrons (i.e., the LDOS),¹² the patterns observed in tunneling electron microscope images arise from an interplay of these two factors. However, the Fowler-Nordheim slope is a derivative of the current-voltage characteristic and essentially independent of the magnitude of the tunneling current. Therefore, the PhotoFEEM barrier maps represent the distribution of tunneling probability across the surface independent of the supply of tunneling electrons. A comparison of FEEM images to their corresponding PhotoFEEM barrier map can be used to determine whether the emission from a particular region is limited by the size of the local tunneling barrier or by the supply of tunneling electrons.⁸

By constructing an appropriate model of the surface electric field, absolute barrier heights can be extracted from a measurement of the Fowler-Nordheim slope. However, because of the complicated nature of the surface charge structure in the presence of a polarizable adsorbate, we have not attempted such an analysis in this work. Regardless, the variations in the Fowler-Nordheim slope can still be considered equivalent to variations in the local tunneling probability. If the surface field strength is roughly constant over the area of interest, which may indeed be the case for small adsorbates, these variations will also be approximately equal to variations in the local barrier height.

We chose CuPc as our target molecule in this work be-

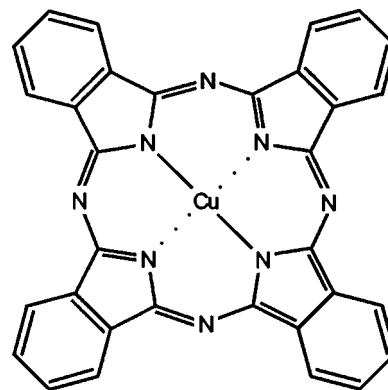


FIG. 2. Kekulé structure of the organic molecule copper-phthalocyanine (CuPc).

cause it has been studied extensively by a variety of surface analytic techniques, including both FEEM and STM, and because of its structural similarity to other interesting molecules such as chlorophyll-a and hemin.¹³ CuPc is a fourfold symmetric compound consisting of a copper atom surrounded by four pyrrole units bound in a porphyrin ring in which two carbon atoms of each pyrrole unit are also part of a benzene ring (Fig. 2). Since the earliest studies in the 1950s, it has been known that CuPc produces several distinctive patterns in the FEEM including well-defined singlets, doublets and quadruplets.^{1,14-16} Given that the dimensions of an individual CuPc molecule are roughly $10 \text{ \AA} \times 10 \text{ \AA}$, the structures observed in these patterns indicate subnanometer resolutions in the FEEM images of this molecule. Although the normal resolving power of the FEEM is approximately 2 nm, the enhanced resolution present in the images of CuPc may be attributed to the decrease in the local radius of curvature due to a small molecule sitting on the emitter surface.^{15,17-20} It has also been suggested that CuPc may adsorb in polymeric stacks¹ and, therefore, the images may correspond to structures significantly larger than a single molecule.

Our apparatus (Fig. 3) consisted of a stainless steel ultra-high vacuum system containing a tungsten field-emitter fac-

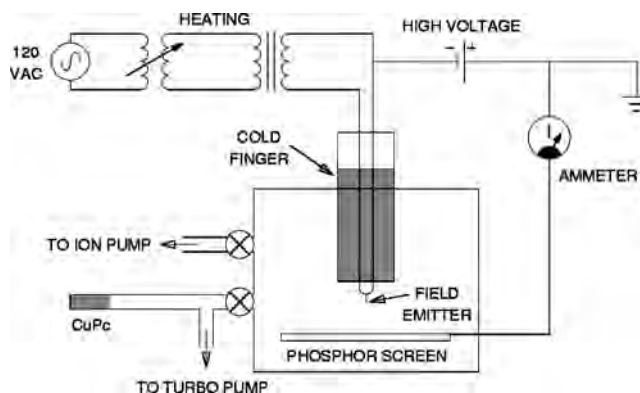


FIG. 3. Schematic of the vacuum system used in the CuPc PhotoFEEM experiments and described in the text. The camera, digitizer, and computer controller were located external to the system and are not shown.

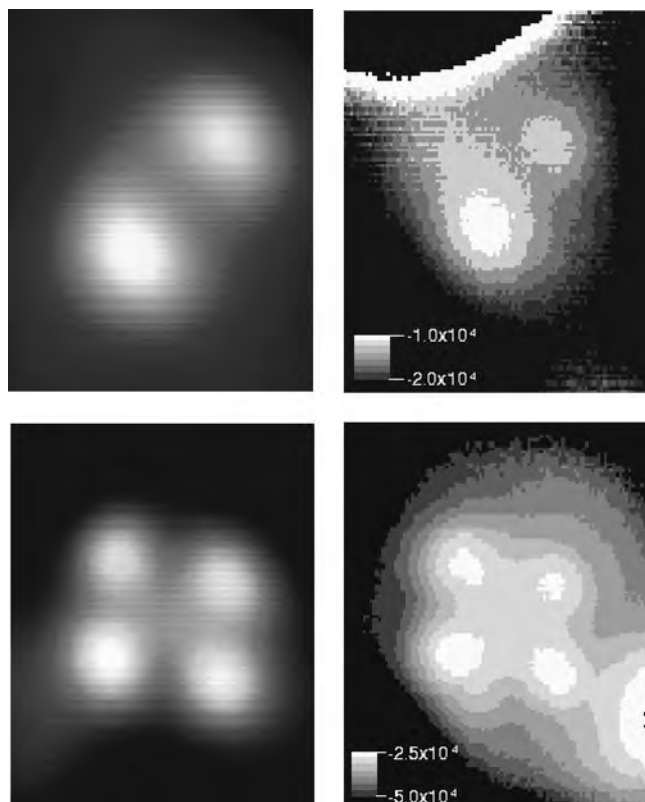


FIG. 4. FEEM images (left) and corresponding barrier maps (right) for a doublet (top) and a quadruplet (bottom) that display the same morphology in both the image and the map. Fowler–Nordheim slope values, in volts, are indicated on the scale bars for the barrier maps.

ing a P-1 phosphor ($\text{Zn}_2\text{SiO}_4:\text{Mn}$) screen settled on a fiber-optic bundle. The CuPc was prepared by repeated sublimation in a quartz sidearm that was evacuated by a dedicated turbomolecular pump and connected to the rest of the system by an all-metal, straight-through valve. After cleaning, the valve was opened and a low-energy molecular beam of the CuPc was admitted into the main chamber where it was deposited on the surface of the emitter. The field emitters were prepared by electrolytic etching of 6 mil tungsten wires in a 1 N NaOH solution and were cleaned and annealed by resistive heating to white heat of a 12 mil molybdenum mounting loop. In order to encourage deposition of the polarizable CuPc molecules at the cathode's apex, the dosing procedure was performed with an electric field applied to the emitter. This approach provided the additional benefit of being able to observe the deposition process in the field-emission image. Unfortunately, repeated dosings and cleanings of the emitter with field applied resulted in surface carbon contamination and significant “build up” of the edges of the close-packed planes.^{1,21} This complicates our observations because of the presence of unknown organic adsorbates, probably thermal decomposition products of CuPc, on the surface. Furthermore, since most small organic adsorbates produce identical FEEM images,²² it is impossible to determine the exact source of the images within the limitations of the FEEM. The buildup of the surface enhances the preferential deposition of the polarizable CuPc

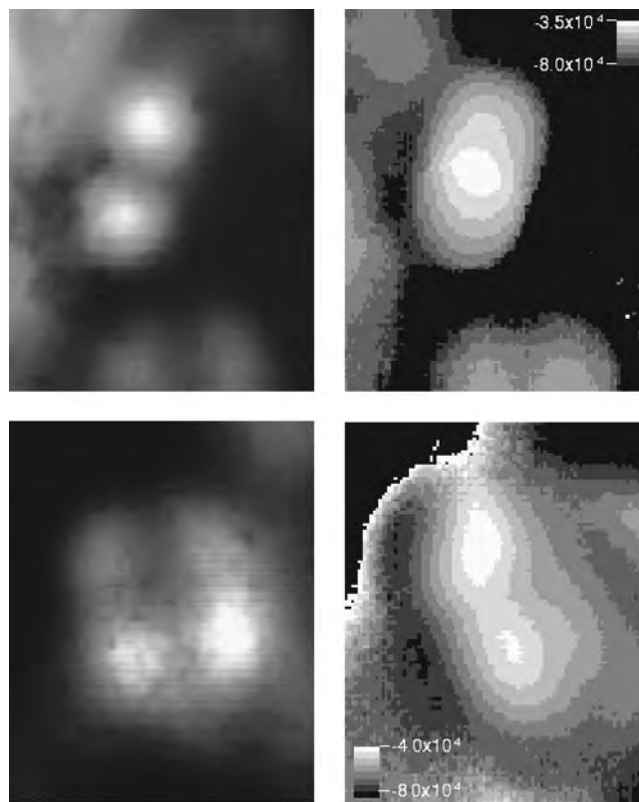


FIG. 5. FEEM images (left) and corresponding barrier maps (right) for a FEEM doublet that displays a singlet in the PhotoFEEM barrier map (top) and a FEEM quadruplet that displays a doublet in the PhotoFEEM barrier map (bottom). Fowler–Nordheim slope values, in volts, are indicated on the scale bars for the barrier maps.

molecules at sharp edges and, as a result, the majority of our data were taken from the edges of the (110) and (211) planes. This produces asymmetries in some of our images due to nonuniform magnification at sharply curved surfaces.

In order to increase the stability and dwell times of the molecular images,¹ the field emitter was cooled by liquid nitrogen and the main chamber was ion pumped to a pressure lower than 10^{-9} Torr for all experiments. Images were captured with an analog charge coupled device (CCD) video camera located external to the system and digitized to 512×512 pixels at 8 bits (256 gray levels). At least 18 video frames were summed for each image in order to increase the dynamic range of the data. The images were then normalized, dark corrected and calibrated for phosphor response as a function of electron energy before analysis.⁸ Precautions were taken to eliminate photometric artifacts including the use of a fiber-optic bundle to reduce the transmission of scattered light and the elimination of long exposure images that displayed low-light CCD nonlinearities. High voltage was provided by a -10 kV power supply and anode currents were measured with a picoammeter to calibrate the response of the phosphor screen. The majority of the data were taken between 3 and 5 kV with a voltage increment of 25 V between images. The entire experiment was controlled by a computer running custom code developed in-house for the PhotoFEEM system.⁸

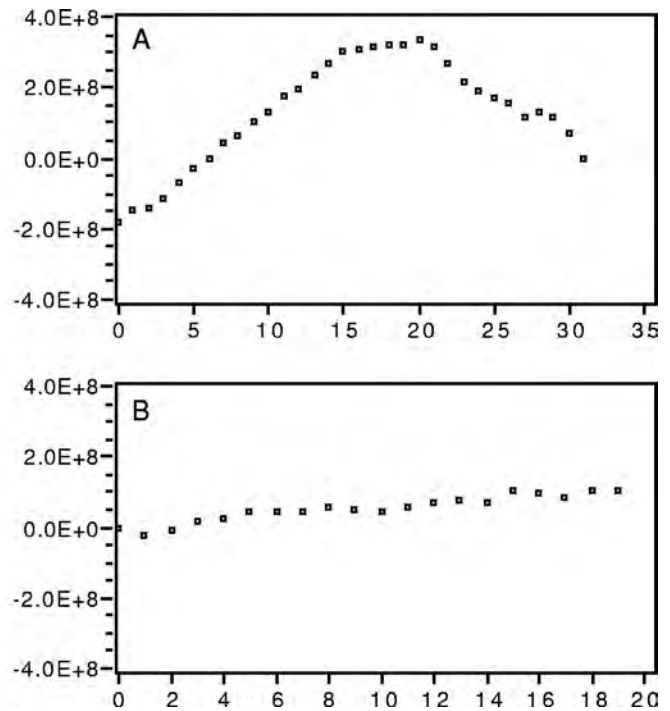
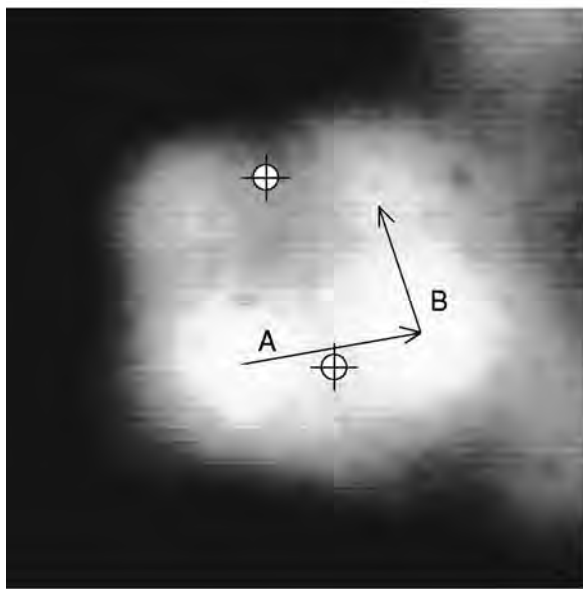


FIG. 6. Curvature in the Fowler–Nordheim coordinates as a function of pixel number (right) for the paths shown on the FEEM image of a quadruplet (left). This quadruplet, also shown in Fig. 2, displays a well-defined doublet in the PhotoFEEM barrier map whose peaks are indicated by crosses on the FEEM image. The curvature was measured as the coefficient of the quadratic term in a second-order polynomial fit to a Fowler–Nordheim plot of $\ln(L/V^2)$ vs $(1/V)$ where L is the photometric luminosity. Note that the curvature is pronounced only where the two states are spatially superimposed in the image.

A total of 27 experiments were performed from which 14 doublet and 18 quadruplet patterns were chosen for analysis. The patterns were selected based on clarity, stability and the presence of the molecule in at least 10 consecutive images. None of the molecular patterns chosen for study displayed any significant structural variations over the set of data images. For each molecular pattern, a 100×100 pixel “barrier map” of the Fowler–Nordheim slope was constructed using the PhotoFEEM technique. Of these patterns, three of the doublets (21%) and eight of the quadruplets (44%) appear identical in the PhotoFEEM barrier map to their appearance in the field-emission images (Fig. 4). Since the tunneling current is primarily determined by the size of the local tunneling barrier, these results are not surprising—one would expect that the regions of greatest emission in the FEEM images would correlate directly with the regions of smallest tunneling barrier measured by the Fowler–Nordheim slope. However, several molecular images displayed very different and surprising behavior (Fig. 5): 6 of the 14 doublets (43%) displayed a singlet structure in the barrier map and 3 of the 18 quadruplets (17%) displayed a doublet structure in the barrier map. In all of these data sets, the minima in the tunneling barrier were located in dark regions of the FEEM patterns. This behavior is quite unexpected—one would expect that a minimum in the tunneling barrier would produce a maximum in the tunneling current. The remaining molecular images, five doublets (36%) and seven quadruplets (39%), display an intermediate behavior in which there are regions of small barrier size in the dark clefts of the FEEM

images but the barrier maps do not possess any well-defined structure.

Our ability to measure the tunneling barrier of low emission areas is fundamentally limited by the minimum luminosity we can detect. The apparent absence of a barrier structure in the dark areas of some data sets may simply be caused by insufficient photometric data in those regions. However, other more interesting possibilities exist. For example, the observed distribution of barrier morphologies may be due to variations in the adsorption conditions among the individual data sets. However, attempts to correlate the different behaviors with different regions of the surface were inconclusive. Another possibility is that, even under the same adsorption conditions, there may be a statistical distribution of barrier types for the adsorbate. An example of this type of effect would be the existence of multiple charge states of the adsorbed molecule. It has been suggested that uncharged CuPc on the surface may not emit¹ and, therefore, this effect could also be related to the unexplained statistical distribution of image types as well. Additional factors, such as coadsorption with surface impurities and CuPc polymerization, may affect our results but could not be evaluated in these experiments. Hopefully, future experiments will be able to identify the principal factors in determining the observed distribution of barrier structures for the different image types of CuPc.

In order to clarify the difference between the structures observed in the FEEM image and the PhotoFEEM barrier map, a further analysis was performed to determine the spatial structure of deviations from purely linear Fowler–

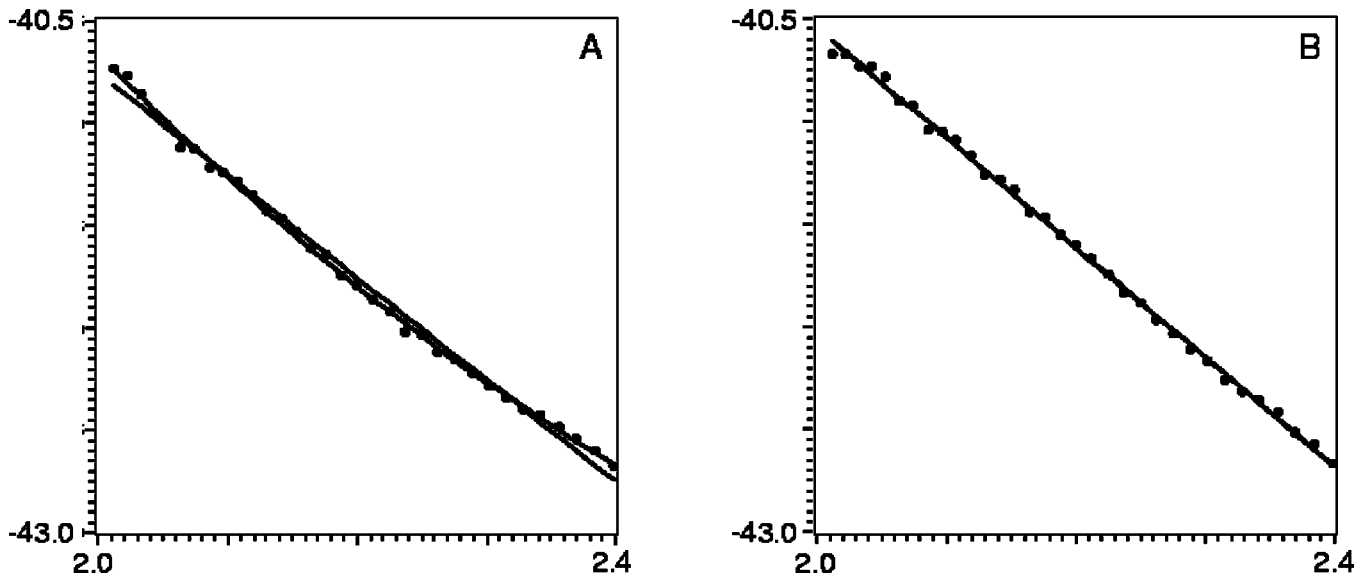


FIG. 7. Fowler–Nordheim plots of $\ln(L/V^2)$ (arb units) vs $(1/V)$ ($\times 10^{-4} \text{ V}^{-1}$) for (A) the pixel exhibiting the maximum curvature in the top trace of Fig. 6 and (B) the pixel exhibiting zero curvature at the junction of the two traces in Fig. 6. The second-order polynomial fit is indicated by the solid curve and the best-fit line by the dashed curve.

Nordheim behavior. When the currents from independent field emitters are measured together, the resulting current–voltage characteristic will not be strictly linear in the Fowler–Nordheim coordinates, $\ln(I/V^2)$ vs $(1/V)$. In fact, the Fowler–Nordheim plot should display a curvature that depends on the distribution of Fowler–Nordheim characteristics contributing to the measured currents.^{10,23} This effect has previously been used to study the adsorption of barium on tungsten²¹ and the distribution of emission characteristics in microfabricated field-emitter arrays.^{24,25} For our analysis, we went back to the original single pixel $\ln(I/V^2)$ vs $(1/V)$ data and, instead of fitting to a straight line as in the traditional Fowler–Nordheim analysis, we fit to a second-order polynomial and used the coefficient of the quadratic term as a measure of the emission’s nonlinearity. Our analysis showed that when different structures were observed in the FEEM image and the PhotoFEEM barrier map, then the curvature was greatest where they were superimposed and approximately zero elsewhere (Fig. 6). In the context of these experiments, this implies that these structures arise from different emitters—possibly different energy states of the adsorbate or different molecules in a coadsorbed complex. It should be noted that even the largest deviations from linearity are quite small (Fig. 7). However, since the linear term should go as the average work function of the two emitters while the quadratic term would go as the difference in work functions,²³ the small observed curvatures would be consistent with emission from two closely spaced energy levels. In order to verify that the observed curvatures were not due to low-light nonlinearities in our imaging system, similar measurements were taken in the dark regions adjacent to the molecular images and the effect was not observed.

III. DISCUSSION

The similarity between the doublets observed in the barrier maps of quadruplet images and the doublets observed in other FEEM images raises the possibility that these structures arise from the same source. Other experiments have already indicated that the emission from CuPc arises from multiple states^{26,27} and that the different image types can be associated with different Fowler–Nordheim slopes.²⁸ In the course of our experiments, a single tantalizing run of data was acquired in which a FEEM quadruplet with a doublet barrier map spontaneously converted to a FEEM doublet with the same orientation as the barrier map doublet as the field strength was increased. Unfortunately, insufficient data were acquired to construct a barrier map for this subsequent FEEM doublet and the effect has proven difficult to reproduce. If indeed these structures can originate from the same source, it would be difficult to describe the different images as arising from different conformations of the adsorbate on the surface. Obviously, investigation of the relationship between the structures observed in the FEEM images and the corresponding barrier maps represents an important area for further research.

The lack of chemical information in tunneling electron micrographs has long been a problem for the interpretation of the resulting images.^{1,2,3,22} Several possible sources for the observed structures have been proposed including molecular orbitals,²⁹ adsorbate ‘‘waveguide’’ states^{30–32} and diffraction patterns³³ but none has been proven unambiguously. While quantum chemical calculations have proven useful in the interpretation of STM images,^{29,34,35} this technique has not generally been applied to FEEM images. However, since these calculations tend to produce only fourfold symmetric

barriers for CuPc,²⁹ the observations reported in this article present a novel challenge for this approach. Ultimately, it will require chemically specific techniques such as atom-probe or any of a number of spectroscopies to answer these questions.

ACKNOWLEDGMENTS

The authors would like to thank Professor David Dunlap for many helpful discussions on this work. This research was supported in part by a graduate fellowship from the Center for Advanced Studies in the Department of Physics and Astronomy at the University of New Mexico.

¹A. J. Melmed and E. W. Müller, *J. Chem. Phys.* **29**, 1037 (1958).

²C. R. Clemmer and T. P. Beebe, *Science* **251**, 640 (1991).

³G. Binnig and H. Rohrer, *IBM J. Res. Dev.* **30**, 355 (1986).

⁴J. K. Spong *et al.*, *Nature (London), Phys. Sci.* **338**, 137 (1989).

⁵M. Kimura *et al.*, *Jpn. J. Appl. Phys., Part 1* **34**, 3642 (1995).

⁶S. Richter and Y. Manassen, *J. Phys. Chem.* **98**, 2941 (1994).

⁷R. G. Forbes, *Scanning Tunneling Microscopy and Related Methods* (Kluwer Academic, Norwell, MA, 1990), p. 163.

⁸G. R. Condon and J. A. Panitz, *J. Vac. Sci. Technol. B* **16**, 23 (1998).

⁹R. H. Fowler and L. W. Nordheim, *Proc. R. Soc. London, Ser. A* **119**, 173 (1928).

¹⁰R. Gomer, *Field Emission and Field Ionization*, American Vacuum Soci-

ety Classes (American Institute of Physics, New York, 1993), p. 48.

¹¹E. C. Teague, *J. Res. Natl. Bur. Stand.* **91**, 171 (1986).

¹²R. D. Young, *Phys. Rev.* **113**, 110 (1959).

¹³F. H. Moser and A. L. Thomas, *Phthalocyanine Compounds* (Reinhold, New York, 1963).

¹⁴E. W. Müller, *Z. Naturforsch. A* **5**, 473 (1950).

¹⁵R. Gomer and D. A. Speer, *J. Chem. Phys.* **21**, 73 (1953).

¹⁶P. Wolf, *Z. Angew. Phys.* **6**, 529 (1954).

¹⁷E. W. Müller, *Z. Phys.* **131**, 136 (1951).

¹⁸R. Gomer, *J. Chem. Phys.* **20**, 1772 (1952).

¹⁹D. J. Rose, *J. Appl. Phys.* **27**, 215 (1956).

²⁰I. Brodie, *Surf. Sci.* **70**, 186 (1978).

²¹E. W. Müller, *Ergeb. Exakten. Naturwiss.* **27**, 290 (1953).

²²R. Haefer, *Acta Phys. Austriaca* **8**, 105 (1953).

²³G. R. Condon, Thesis, University of New Mexico, 1999, Appendix B.

²⁴N. A. Cade *et al.*, *J. Vac. Sci. Technol. B* **13**, 549 (1995).

²⁵J. D. Levine, *J. Vac. Sci. Technol. B* **13**, 553 (1995).

²⁶L. W. Swanson and L. C. Crouser, *Surf. Sci.* **23**, 1 (1970).

²⁷W. Mizutani *et al.*, *J. Vac. Sci. Technol. A* **8**, 675 (1990).

²⁸H. Morikawa *et al.*, *Jpn. J. Appl. Phys., Part 2* **36**, L583 (1997).

²⁹P. Sautet and C. Joachim, *Surf. Sci.* **271**, 387 (1992).

³⁰A. P. Komar and A. A. Komar, *Sov. Phys. Tech. Phys.* **6**, 166 (1961).

³¹A. P. Komar and A. A. Komar, *Sov. Phys. Tech. Phys.* **7**, 634 (1963).

³²A. P. Komar and A. A. Komar, *Sov. Phys. Solid State* **7**, 606 (1965).

³³R. Gomer, *J. Chem. Phys.* **19**, 1072 (1951).

³⁴H. Ohtani *et al.*, *Phys. Rev. Lett.* **60**, 2398 (1988).

³⁵P. H. Lippel *et al.*, *Phys. Rev. Lett.* **62**, 171 (1989).